GOSPODARKA SUROWCAMI MINERALNYMI – MINERAL RESOURCES MANAGEMENT

2024 Volume 40 Issue 2 Pages 89–119

DOI: 10.24425/gsm.2024.150829

IWONA JONCZY[1], KRZYSZTOF FILIPOWICZ[2]

# The use of scanning electron microscopy in the study of the components of Zn-Pb slags on the example of slags from the dump in Bykowina (Ruda Śląska)

## Introduction

In Upper Silesia, the area of today's city of Ruda Śląska is one of the examples of a Zn-Pb industry development center. Metal ores were exploited here as far back as in the early Middle Ages, but the settlement really flourished at the turn of the eighteenth and nineteenth century. The metallurgical waste dumps remaining in the city date back to this period (Dworak and Ratka 1985; Dworak 1995; Jonczy 2022). At the beginning, weathered Zn-Pb ores (galmei) were exploited and smelted. Galmei ores represent a mixture of zinc oxides and silicates, dolomite and iron oxides and occur on the surface or at shallow depths so do not cause any problems during mining. There are two types of galmei: white and red –

✉ Corresponding Author: Iwona Jonczy; e-mail: iwona.jonczy@polsl.pl

[1] Silesian University of Technology, Faculty of Mining, Safety Engineering and Industrial Automation, Gliwice, Poland; ORCID iD: 0000-0003-2635-8484; e-mail: iwona.jonczy@polsl.pl

[2] Silesian University of Technology, Faculty of Mining, Safety Engineering and Industrial Automation, Gliwice, Poland; ORCID iD: 0000-0001-6672-1378; e-mail: krzysztof.filipowicz@polsl.pl

rich in iron oxides (mainly hematite). Like in the whole Upper Silesia, the development of the zinc industry in Ruda Śląska took place in the eighteenth and nineteenth century, which was the result of using increasingly advanced mining technologies enabling the exploitation of deeper sulfide ores. Rich in zinc and lead sulfides, this raw material led to the establishment of numerous galvanizing plants in Ruda. They were, among others: Miłość, Karol, Godula, Hugo, Zorza Poranna, Dobra Nadzieja, Rozamunda; most of them began to operate in the years 1812–1842 and functioned until the nineteen-thirties. What is left of their operations are waste dumps (Pazdur 1961; Popiołek 1965).

The technology of processing sulfide ores consisted of roasting the blend and further processing in distillation furnaces. An important moment in zinc production technology was the development of the hydrometallurgical method (1880–1881), while in the nineteen-thirties, zinc production was based mainly on pyrometallurgical technology. In the years 1931–1935, a method for refining zinc was developed in the United States, and in the nineteen-fifties, a technology for the simultaneous production of zinc and lead in one production cycle, ISP (imperial smelting process) was developed. In Poland, the method based on the ISP shaft furnace was used in the nineteen-sixties; its use in the steelworks in Miasteczko Śląskie replaced metallurgical plants with muffle furnaces (Popiołek 1965).

The use of modern technologies of zinc ore exploitation and processing caused the zinc industry to develop on a large scale. However, the metallurgical process was accompanied by the generation of a significant amount of waste, especially metallurgical slag, which was initially not subject to any recycling. The slag was stored on dumping grounds without any plan or security for the storage site. To this day, traces of Zn-Pb ore metallurgy can be found in Upper Silesia, including in the remains of former works buildings, but above all, these are metallurgical slag dumps. Currently, as part of various pro-ecological programs, numerous activities are conducted aimed at, firstly, recovering areas occupied by dumping sites or integrating them into the surrounding landscape, and secondly, checking the possibilities of the economic use of Zn-Pb slags.

Zn-Pb slags are a unique group of waste due to a differentiated phase composition as also different degree of components crystallization, which depends on the external conditions of cooling the slag melt. Phase composition mainly depends on the composition of the charge material including the type of additives and fluxing agents (Kucha et al. 1996; Cabała et al. 2008; Ettler et al. 2009; Bleiwas and DiFrancesco 2010; Lin et al. 2015). In chemical composition, Zn-Pb slags often contain significant amounts of heavy metals (including Zn, Pb, Cd) accompanied by a certain amount of sulfides, which are oxidized to sulfates during the long-term storage of waste in dumps. Sulfates migrate with atmospheric waters flowing around the dump, as well as with solutions infiltrating the dump (which is generally facilitated by the porous texture of the slags). Sulfates contribute to the acidification of the environment, which creates favorable conditions for the release and migration of heavy metals. In her works, Kicińska (2021) proves that large quantities of the slag in waste dumps may become an anthropogenic source of elements to be used in the future. However, at present they require protection against leaching and the washing out of the finest particles.

The presence of metals and sulfur in Zn-Pb slags is often an obstacle to its use, inter alia, as a material for the production of aggregates. Additionally, the high degree of weathering of these slags causes them to crumble easily and their physico-mechanical properties are much lower than those of, for example, steel slags, which are successfully used to produce various types of aggregates.

Work on how to use Zn-Pb slags is still ongoing, but it seems that a good alternative to old Zn-Pb slag dumps is their protection and management. These types of activities have been and continue to be conducted in the dumping grounds in Ruda Śląska, which are an example of a well-planned and successful revitalization. One of the dump reclamation process involved phytostabilization – additives reducing the bioavailability of heavy metals were added to the soil and then, selected species of grass with the ability to hold contaminants in the roots were sown. As a result of this, the dump was transformed into a safe, green public space, with a network of walking alleys, resting places, playgrounds and a viewpoint at the top.

All activities related to the use of Zn-Pb slags require detailed knowledge of this material. This especially applies to slags, which are a relic of metallurgy from the last century. Therefore, the analysis of the slag components requires the application of several, complementary research techniques (Jonczy and Stanek 2013, Jonczy 2016, 2018). In the case of this type of waste, the analysis of the phase and chemical composition is difficult because there is often no preserved historical information about the composition of the metallurgical charge and the smelting technology. An additional difficulty is the degree of weathering of the slags – during long-term storage, the phase components and glaze undergo significant transformations. Due to the analysis of the mineralogical composition of slags, it is necessary to use a number of research techniques that will enable a precise understanding of this material. One of them is scanning electron microscopy. SEM, because of the possibility of obtaining high-resolution images of sample surfaces by recording secondary electrons (SE) or backscattered electrons (BSE) characterized by depth of field and high resolution (Koga et al. 2021; Ali et al. 2023; Łydżba-Kopczyńska et al. 2024), which is used in a wide range when testing various materials (Nadeau and Herguth 2004; Liu et al. 2010; Wu et al. 2017; Nocoń et al. 2023), especially during mineralogical research (Zdera 2013).

In this work, the authors focused on researching the phase composition of Zn-Pb slags from the old dump in Ruda Śląska using scanning electron microscopy. Moreover, the aim of the work was to compare the results of determining the phase composition of slags using SEM with the results of XRD analysis.

## 1. Characteristics of research area and material

The tests were conducted on samples taken from an unsecured waste dump on the border of two cities, Ruda Śląska and Świętochłowice. The dump is located in the eastern part of Ruda Śląska, in the Bykowina district (Figure 1). Until the end of the seventeenth century,

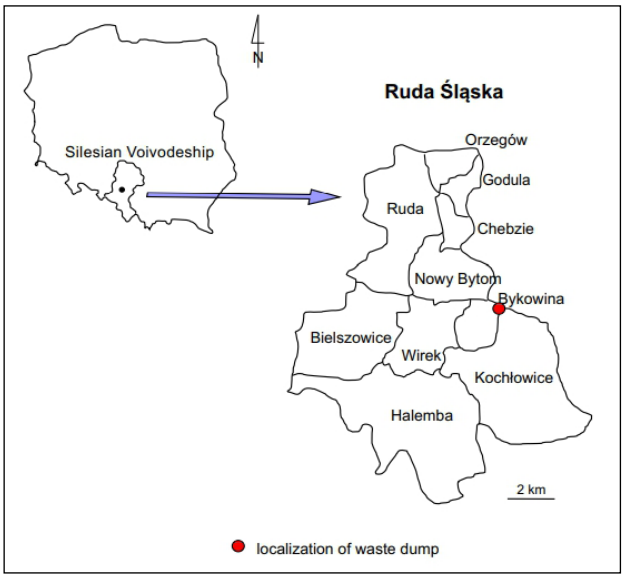


Fig. 1. Sketch with the location of Ruda Śląska (Ruda Śląska Location 2023)

Rys. 1. Szkic z lokalizacją Rudy Śląskiej

Fig. 2. Exposed slope of zinc waste dump in Ruda Śląska – Bykowina (photo A. Bartela)

Rys. 2. Odsłonięta skarpa zwałowiska odpadów pocynkowych w Rudzie Śląskiej – Bykowinie (fot. A. Bartela)

the Bykowina settlement had been a hamlet of Kochłowice, until Donnersmarck founded a village there, originally named Dębowa Kłoda and later – Bykowina. In 1950, Bykowina was joined to the city of Nowy Bytom and in 1959, it became a district of Ruda Śląska. The material stored in the dump is waste from the Franz zinc plant, which operated in this region in the period 1876–1929 and was transformed into a porcelain factory in the interwar period (Popiołek 1965; Dworak and Ratka 1985; Dworak 1995).

Samples were taken from the exposed slope of the dump part located in the Bykowina district of Ruda Śląska. A total of thirty samples were collected from the exposed slopes of the dump (Figure 2).

The material stored in the dump consisted of highly weathered metallurgical slags after zinc and lead production, among which, three types were identified based on their macroscopic features (Figure 3 a–c). Slag 1 was characterized by a red-brown color, medium-sized grains and porous texture. Slag 2 was dark grey, fine-grained and its texture was massive, with a porous texture encountered only locally. Slag 3 was brown-grey, with a fine to medium grain structure and porous texture.


Fig. 3. a–c .Slag samples from waste dump in Ruda Śląska – Bykowina
a) slag 1; b) slag 2; c) slag 3 (photo I. Jonczy)

Rys. 3. a–c. Próbki żużli ze zwałowiska w Rudzie Śląskiej – Bykowinie
a) żużel nr 1; b) żużel nr 2; c) żużel nr 3 (fot. I. Jonczy)

## 2. Methods

The laboratory tests involved microscopic observations using scanning electron microscopy. The scanning electron microscopy tests were performed using a Mira III high-definition scanning microscope manufactured by Tescan equipped with an X-ray microanalysis system (based on energy dispersive X-ray spectrometry EDS) Aztek Automated produced by Oxford Instruments. SEM observations and photographs were made in micro-areas as both fracture and micro-section. Microphotographs were taken at a magnification from 20× to 10,000× using a BSE or SE detector. BSE backscattered electron images were taken for thin samples and secondary electron SEM images were taken for bulk preparations. Prior to the test, the preparations were dusted with carbon.

## 3. Results

Observations by means of scanning electron microscope revealed a fairly high level of porosity for all of the slags in question. Numerous, spherical pores of different sizes were identified. The distribution of the pores in the samples was not uniform; there were highly porous micro-areas as well as places with a low number of pores. Individual samples often showed alternating, layered distribution of micro-areas with and without pores (Figure 4. a, b).

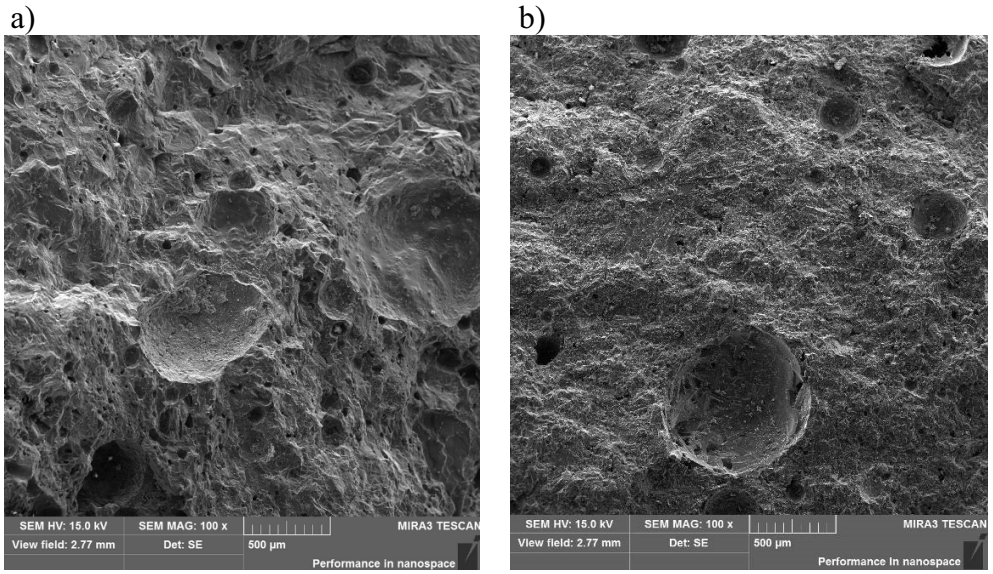


Fig. 4. a, b. Slag surface with visible pores (SE, magnification 100×)

Rys. 4. a, b. Powierzchnia żużla z widocznymi porami (SE, powiększenie 100×)

The presence of pores was connected with the occurrence of layers of liquid material rich in gas components in the slag alloy. As a result of rapid cooling and setting, the slag alloy undergoes degassing, this results in the presence of numerous pores in the slag. It was observed that some pores were filled with recrystallizing minerals from the group of sulfates, carbonates and oxides. In all types of slag, the presence of numerous micro-cracks (usually occurring within the glaze) was also observed (Figure 5).

Several micro-areas were identified in **slag 1** that were vastly differing in chemical composition and phase component formation.

In the first analysed micro-area (Figure 6, Table 1), spinel crystallites could be observed that were rich in Fe, Al and Mg (points 92, 95), characterized by irregular shapes and fuzzy edges within which iron spinel crystallites were clearly visible (points 91, 94) (Figure 7. a, b).

It can be assumed that these were the alloy demixing zones. The analysis of the microphotograph around measuring point 94 showed a clear, sharp line dividing a single spinel

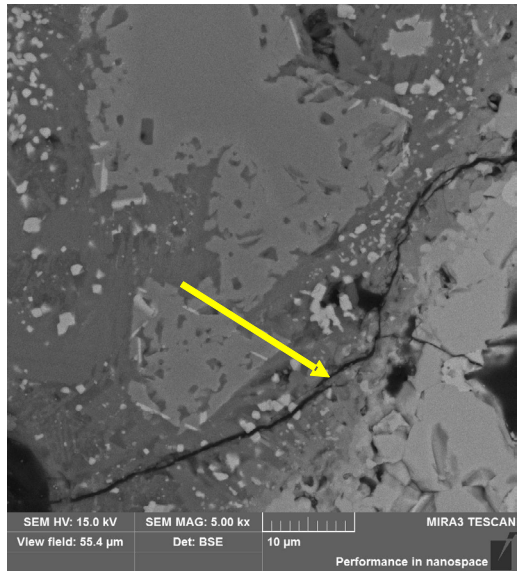


Fig. 5. Micro-cracks occurred within the glaze (BSE, magnification 5,000×)

Rys. 5. Mikrospękania występujące w obrębie szkliwa (BSE, powiększenie 5000×)

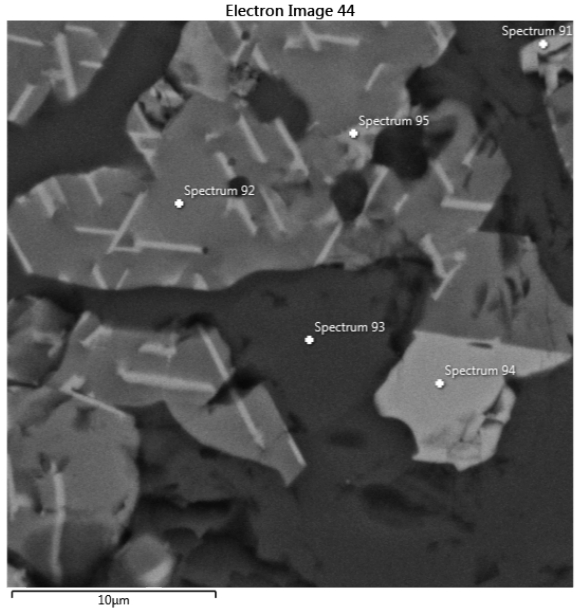


Fig. 6. Microphotograph 1 (BSE, magnification 1,000×) – slag 1

Rys. 6. Mikrofotografia 1 (BSE, powiększenie 1000×) – żużel nr 1

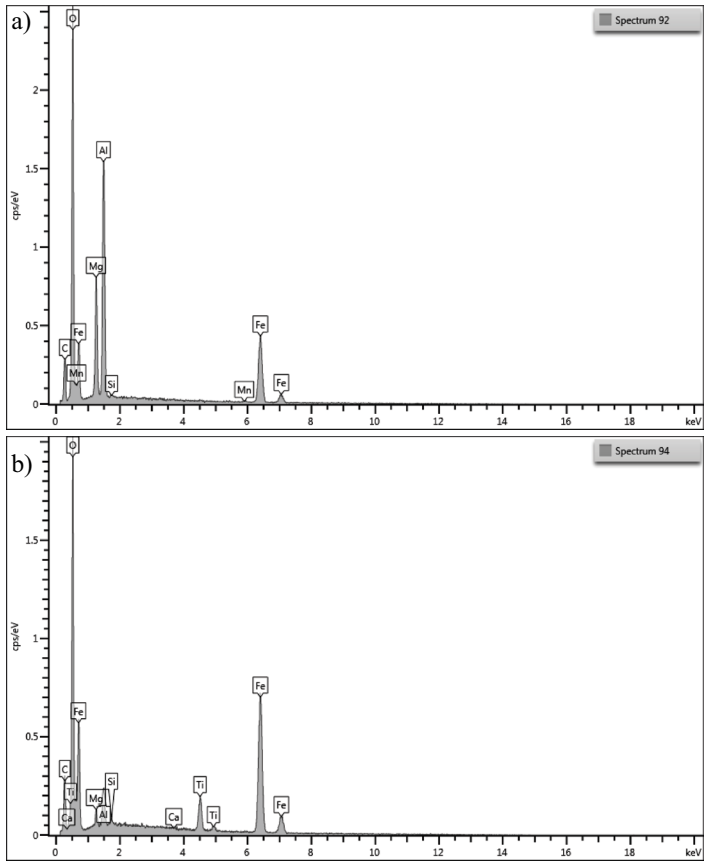


Fig. 7. a, b. EDS spectra of spinels – spectrum 92 and 94, slag 1

Rys. 7. a, b. Widma EDS spineli – widma nr 92 i 94, żużel nr 1

crystallite in two zones: rich in Fe, Al and Mg, and the zone containing mainly Fe with only minor admixtures of other elements. The crystallites were surrounded by glaze (point 93) consisting mainly of Si, Al, Ca, with Fe, Na and K admixtures.

In the other analyzed micro-area (Table 2, Figure 8), there was a significant portion of glaze (point 99); its chemical composition was similar to that of the glaze from the first micro-area.

The major components were Si, Al and Ca, with Na and K admixtures. Compared to the chemical composition of the glaze from the first micro-area, there was no Fe, but instead, Mg admixture was identified. Surrounding the glaze, there were fairly big, well-formed crystals of spinel rich in Al, Fe and Mg (point 102, Figure 8 and Figure 9), and fine crystallites of Fe-Mg silicates (points 100, 101, 103, 104). Substitutions of other elements in their inner structure, inter alia, Ti, could not be ruled out. The content of this element in the chemical composition of individual crystallites might exceed 8% (point 104).

Table 1. Share of elements in measuring points according to Figure 6

Tabela 1. Skład pierwiastkowy w punktach pomiarowych zgodnie z rysunkiem 6

| Element | Content (mass %) | | | | |
|---|---|---|---|---|---|
| | Spectrum 91 | Spectrum 92 | Spectrum 93 | Spectrum 94 | Spectrum 95 |
| O | 35.30 | 33.49 | 43.98 | 29.33 | 31.75 |
| Na | 0.50 | – | 0.51 | – | – |
| Mg | 0.88 | 9.64 | – | 1.28 | 6.08 |
| Al | 6.36 | 18.77 | 18.76 | 2.57 | 11.69 |
| Si | 8.42 | 0.19 | 21.34 | 0.25 | 0.25 |
| K | 0.70 | – | 0.24 | – | – |
| Ca | 1.57 | – | 13.43 | 0.22 | – |
| Ti | 4.04 | – | – | 5.67 | 1.66 |
| Mn | – | 0.58 | – | – | – |
| Fe | 42.22 | 37.32 | 1.74 | 60.67 | 48.56 |
| Total | 100.00 | 100.00 | 100.00 | 100.00 | 100.00 |

Table 2. Share of elements in measuring points according to Figure 8

Tabela 2. Skład pierwiastkowy w punktach pomiarowych zgodnie z rysunkiem 8

| Element | Content (mass %) | | | | | |
|---|---|---|---|---|---|---|
| | Spectrum 99 | Spectrum 100 | Spectrum 101 | Spectrum 102 | Spectrum 103 | Spectrum 104 |
| O | 45.40 | 36.10 | 35.23 | 39.22 | 35.69 | 39.71 |
| Na | 0.64 | – | – | – | – | – |
| Mg | 0.13 | 13.94 | 15.05 | 10.24 | 17.07 | 6.78 |
| Al | 17.98 | 0.49 | 0.91 | 35.50 | 0.06 | 5.24 |
| Si | 23.35 | 16.61 | 17.98 | 0.66 | 18.23 | 15.70 |
| P | – | 0.26 | – | – | – | 0.25 |
| K | 0.92 | 0.28 | 0.19 | – | – | 1.82 |
| Ca | 11.59 | 0.30 | 0.16 | – | – | 0.39 |
| Ti | – | 2.37 | 0.32 | 0.30 | – | 8.46 |
| V | – | – | – | 0.50 | – | – |
| Mn | – | 1.01 | 0.83 | – | 0.78 | 0.34 |
| Fe | – | 28.64 | 29.34 | 13.58 | 28.17 | 21.30 |
| Total | 100.00 | 100.00 | 100.00 | 100.00 | 100.00 | 100.00 |

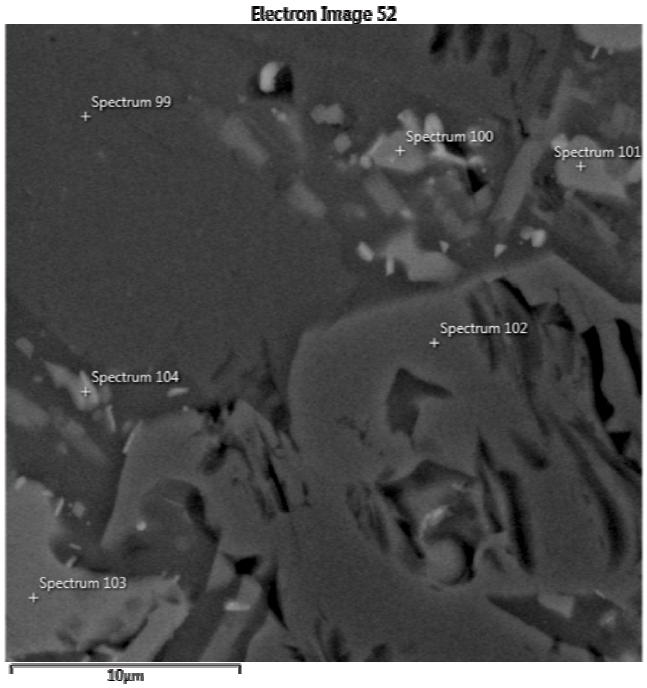


Fig. 8. Microphotograph 2 (BSE, magnification 1,000×) – slag 1

Rys. 8. Mikrofotografia 2 (BSE, powiększenie 1000×) – żużel nr 1

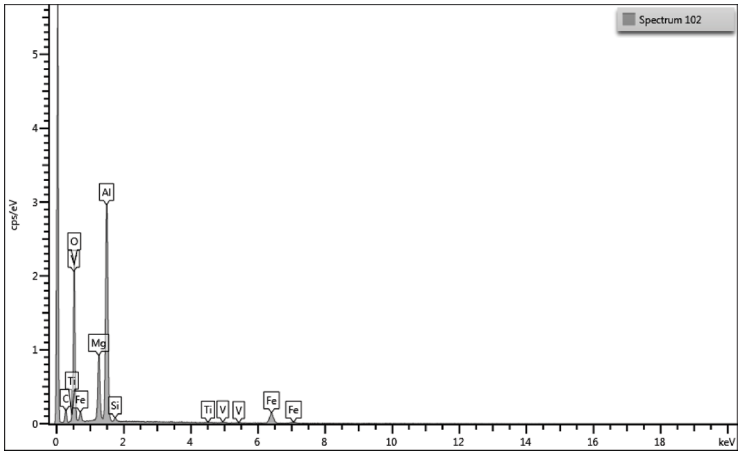


Fig. 9. EDS spectra of spinel rich in Al, Fe and Mg – spectrum 102, slag 1

Rys. 9. Widma EDS spineli bogatych w Al, Fe i Mg – widmo nr 102, żużel nr 1

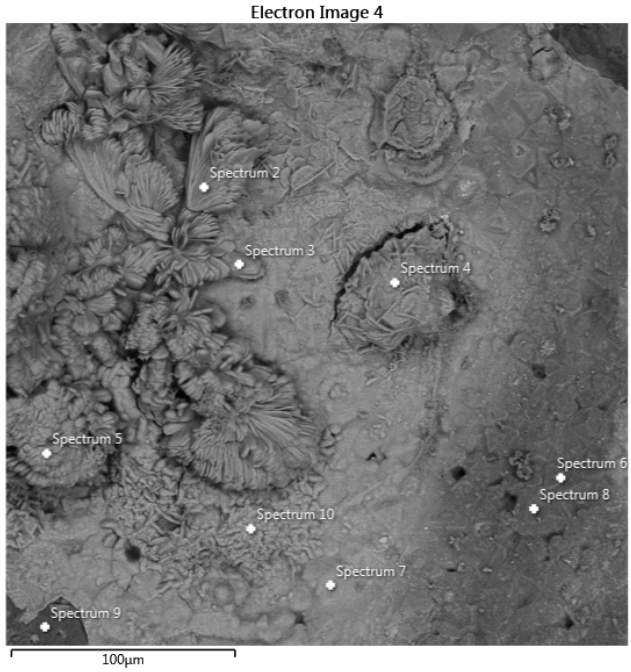


Fig. 10. Microphotograph 3 (SE, magnification 1,000×) – slag 1

Rys. 10. Mikrofotografia 3 (SE, powiększenie 1000×) – żużel nr 1

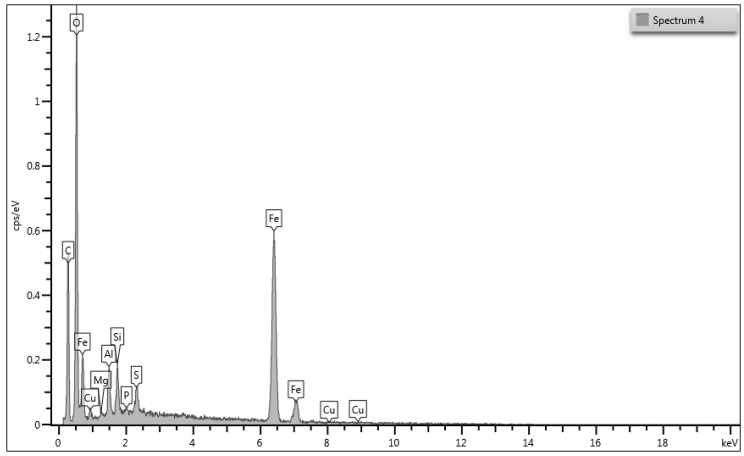


Fig. 11. EDS spectrum – spectrum 4, slag 1

Rys. 11. Widmo EDS – widmo nr 4, żużel nr 1

The pores identified in the tested slags were often filled with recrystallizing minerals. Microphotographs 10 and 11 and also Table 3 shows a crystalline concentration of iron oxide which fills the space created during the degassing of the slag alloy.

Barite was also one of the secondary minerals crystallizing in the waste dump (Figure 12. a b, Figure 13, Table 4) which crystallized as fine plates on the slag surface or in the pores (points 25, 26).

Table 3. Share of elements in measuring points according to Figure 10

Tabela 3. Skład pierwiastkowy w punktach pomiarowych zgodnie z rysunkiem 10

| Element | Content (mass %) | | | | | | | | |
|---|---|---|---|---|---|---|---|---|---|
| | Spectrum 2 | Spectrum 3 | Spectrum 4 | Spectrum 5 | Spectrum 6 | Spectrum 7 | Spectrum 8 | Spectrum 9 | Spectrum 10 |
| O | 42.62 | 43.90 | 23.78 | 1.29 | 46.34 | 36.24 | 37.95 | 36.12 | 15.94 |
| Mg | – | – | 0.30 | – | 11.43 | 0.48 | 11.57 | 13.37 | 0.24 |
| Al | 1.71 | 2.26 | 2.77 | 0.31 | 30.18 | 3.04 | 31.99 | 34.81 | 1.61 |
| Si | 1.83 | 1.66 | 2.45 | – | 1.63 | 2.02 | 1.38 | 0.76 | 1.66 |
| P | 0.33 | 0.41 | 0.21 | – | 0.15 | 0.24 | – | – | – |
| S | 1.21 | 1.30 | 1.50 | – | 0.08 | 1.05 | 0.23 | – | 0.68 |
| Fe | 52.30 | 50.48 | 66.13 | 98.39 | 10.19 | 56.93 | 16.89 | 14.94 | 79.87 |
| Cu | – | – | 2.87 | – | – | – | – | – | – |
| Total | 100.00 | 100.00 | 100.00 | 100.00 | 100.00 | 100.00 | 100.00 | 100.00 | 100.00 |

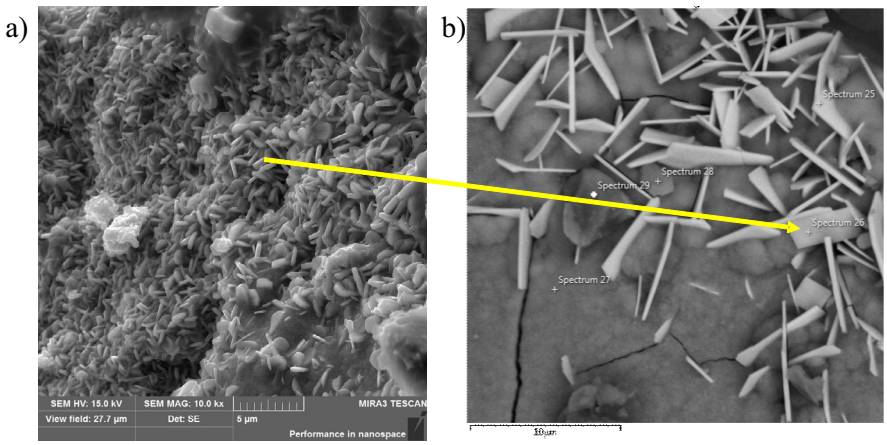


Fig. 12. a, b. Microphotograph 4 a, b (SE, magnification a) 500×, b) 1,000× ) – slag 1

Rys. 12. a, b. Mikrofotografia 4 a, b (SE, powiększenie a) 500×, b) 1000×) – żużel nr 1

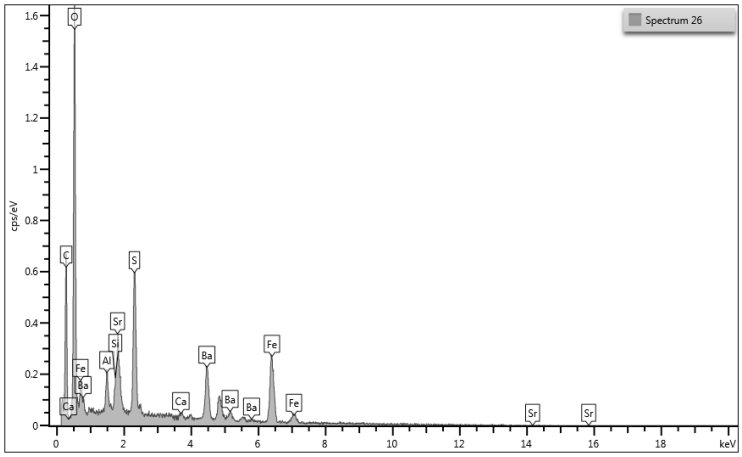


Fig. 13. EDS spectrum – spectrum 26, slag 1 (point 26, according to Figure 12b)

Fig. 13. Widmo EDS – widmo nr 26, żużel nr 1 (punkt 26, zgodnie z rysunkiem 12b)

Table 4. Share of elements in measuring points according to Figure 12

Tabela 4. Skład pierwiastkowy w punktach pomiarowych zgodnie z rysunkiem 12

| Element | Content (mass %) | | | | |
|---|---|---|---|---|---|
| | Spectrum 25 | Spectrum 26 | Spectrum 27 | Spectrum 28 | Spectrum 29 |
| O | 39.74 | 31.79 | 47.11 | 41.42 | 56.55 |
| Na | – | – | – | – | 0.53 |
| Mg | – | – | – | – | 0.23 |
| Al | 1.36 | 2.08 | 5.51 | 4.40 | 6.88 |
| Si | 1.04 | 1.35 | 2.81 | 3.10 | 23.91 |
| P | – | – | – | – | 0.18 |
| S | 11.50 | 9.18 | 1.81 | 2.35 | 0.61 |
| K | – | – | – | – | 4.74 |
| Ca | 0.44 | 0.48 | – | – | 2.11 |
| Ti | – | – | – | – | 0.99 |
| Fe | 7.62 | 25.03 | 42.77 | 45.73 | 3.27 |
| Zn | 0.17 | – | – | – | – |
| Sr | 9.86 | 7.60 | – | 1.02 | – |
| Ba | 28.27 | 22.49 | – | 1.98 | – |
| Total | 100.00 | 100.00 | 100.00 | 100.00 | 100.00 |

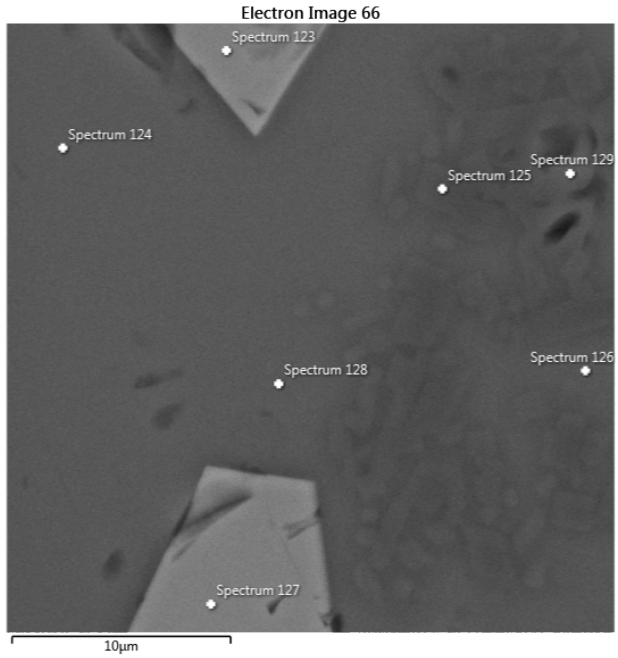


Fig. 14. Microphotograph 1 (BSE, magnification 5,000×) – slag 2

Rys. 14. Mikrofotografia 1 (BSE, powiększenie 5000×) – żużel nr 2

Table 5. Share of elements in measuring points according to Figure 14

Tabela 5. Skład pierwiastkowy w punktach pomiarowych zgodnie z rysunkiem 14

| Element | Content (mass %) | | | | | | |
|---|---|---|---|---|---|---|---|
| | Spectrum 123 | Spectrum 124 | Spectrum 125 | Spectrum 126 | Spectrum 127 | Spectrum 128 | Spectrum 129 |
| O | 34.76 | 49.38 | 48.02 | 49.17 | 34.28 | 47.85 | 50.14 |
| Na | 2.07 | 0.79 | 0.11 | 0.73 | 2.21 | 0.84 | 0.61 |
| Mg | 3.01 | 0.10 | 0.14 | 0.20 | 2.80 | 0.34 | 0.15 |
| Al | 30.98 | 7.72 | 33.86 | 9.40 | 31.17 | 9.16 | 13.07 |
| Si | 0.27 | 34.02 | 16.18 | 32.92 | 0.27 | 31.22 | 29.39 |
| K | – | 4.16 | 0.21 | 3.66 | – | 3.81 | 3.20 |
| Ca | – | 1.74 | – | 1.72 | – | 1.54 | 1.39 |
| Ti | – | 0.87 | 0,53 | 0,96 | – | 0.83 | 0.92 |
| Fe | 6.47 | 1.23 | 0.95 | 1.23 | 6.49 | 1.78 | 1.12 |
| Zn | 22.43 | – | – | – | 22.77 | 2.64 | – |
| Total | 100.00 | 100.00 | 100.00 | 100.00 | 100.00 | 100.00 | 100.00 |

In **slag 2**, the presence of Al-Zn spinel ($ZnAl_2O_4$ gahnite) was clearly distinguishable (Figure 14, Table 5 and Figure 15). Gahnite crystals were well developed, idiomorphic and had a characteristic octahedral habit (points 123, 127). In the analyzed micro-area, poorly developed aluminum silicate crystallites were identified (points 125, 129), surrounded by silicate glaze (points 124, 126, 128).

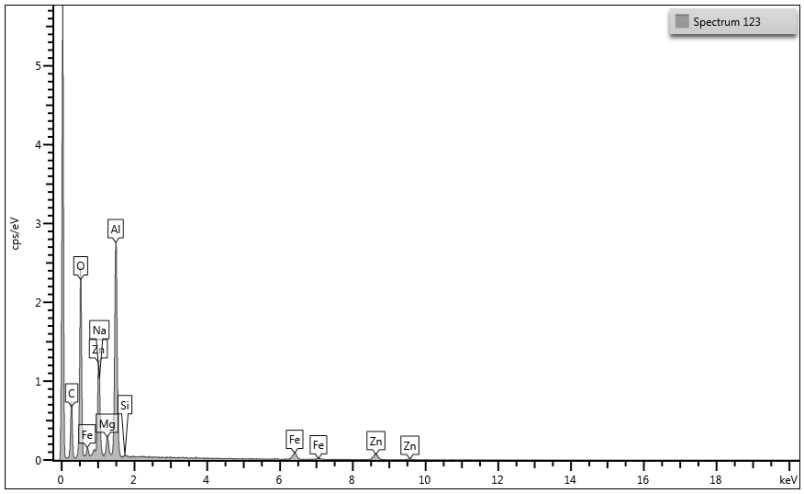


Fig. 15. EDS spectrum – spectrum 123, slag 2

Rys. 15. Widmo EDS – widmo nr 123, żużel nr 2

In the micro-area presented in Figure 16 (Figure 16, Table 6), there were idiomorphic, well-formed aluminosilicate crystallites: rich in Ti (points 152, 154) and K (points 151, 156). Near them, a prolonged crystallite of spinel rich in Fe and Al was identified (point 153) (Figure 17). The crystalline phases were surrounded by silicate glaze (point 155).

The slag had visible pores (Figure 18. a, b, Table 7) filled with isometric Al-Fe spinel crystals with heavy metal substitutions: Cu and Zn (points 49, 53). Between them, there were fine Fe-Cu oxide crystallites (points 48, 52) (Figure 19) as well as almost pure Cu oxide (point 54). Single $SiO_2$ crystals (point 51) were observed. Crystalline phases occurred surrounded by glaze rich in Si, Al, Fe and Ca (point 50).

In **slag 3**, in the micro-area presented in Figure 20 (Figure 20, Table 8), there was glaze (points 213, 215) and clearly visible spherical Fe oxide precipitates (point 218) with Fe sulfate (point 216) (Figure 21). Very fine, point precipitates of Ti oxide (point 220) and Fe oxide (point 217) could be identified in the glaze, as well as crystallites with needle-like habit rich in Al and Si (point 219), which indicated the presence of mullite. Point 214 indicated the presence of gypsum.

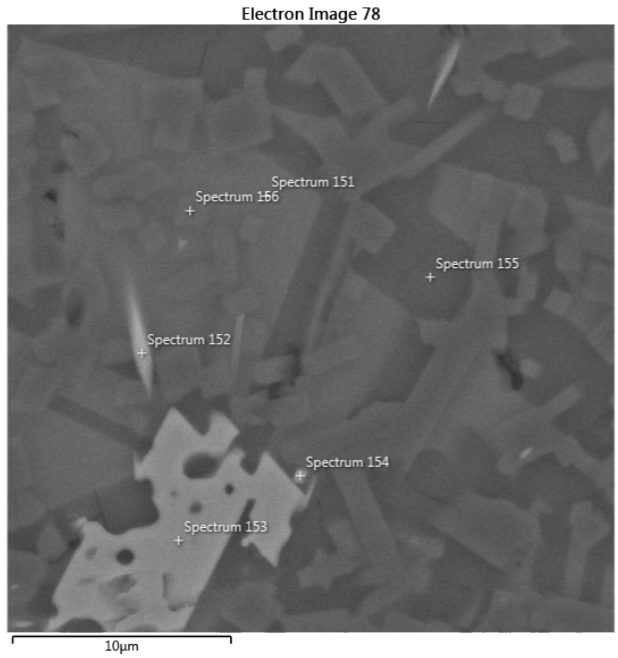


Fig. 16. Microphotograph 2 (BSE, magnification 5,000×) – slag 2

Rys. 16. Mikrofotografia 2 (BSE, powiększenie 5000×) – żużel nr 2

Table 6. Share of elements in measuring points according to Figure 16

Tabela 6. Skład pierwiastkowy w punktach pomiarowych zgodnie z rysunkiem 16

| Element | Content (mass %) | | | | | |
|---|---|---|---|---|---|---|
| | Spectrum 151 | Spectrum 152 | Spectrum 153 | Spectrum 154 | Spectrum 155 | Spectrum 156 |
| O | 50.28 | 50.00 | 37.20 | 51.02 | 53.44 | 49.20 |
| Na | 0.62 | 0.18 | 1.37 | – | 0.13 | 0.25 |
| Mg | 0.21 | – | 4.08 | 0,53 | – | 0.12 |
| Al | 8.88 | 5.96 | 30.63 | 7.62 | 1.05 | 28.64 |
| Si | 32.01 | 13.36 | 0.79 | 12.44 | 44.92 | 18.82 |
| P | 0.16 | – | – | 0.00 | – | – |
| K | 3.89 | 0.73 | – | 0.45 | 0.09 | 0.72 |
| Ca | 1.46 | 0.25 | – | 0.23 | – | 0.26 |
| Ti | 1.00 | 28.28 | – | 23.71 | 0.37 | 0.68 |
| Fe | 1.49 | 0.59 | 13.52 | 1.41 | – | 1.31 |
| Zn | – | – | 12.41 | 1.93 | – | – |
| Zr | – | 0.65 | – | 0.65 | – | – |
| Total | 100.00 | 100.00 | 100.00 | 100.00 | 100.00 | 100.00 |

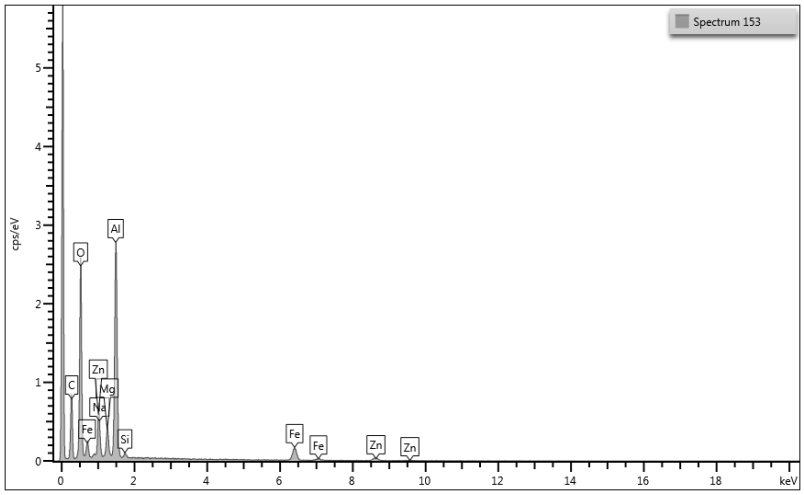


Fig. 17. EDS spectrum – spectrum 153, slag 2

Rys. 17. Widmo EDS – widmo nr 153, żużel nr 2

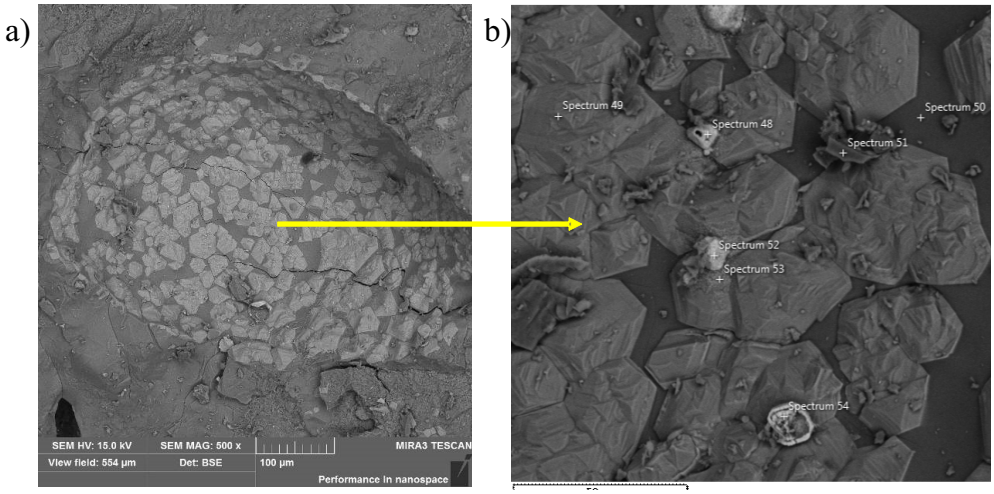


Fig. 18. a, b. Microphotograph 2 a, b (SE, magnification a) 500x, b) 2,000×) – slag 2

Rys. 18. a, b. Mikrofotografia 2 a, b (SE, powiększenie a) 500x, b) 2000×) – żużel nr 2

Table 7. Share of elements in measuring points according to Figure 18

Tabela 7. Skład pierwiastkowy w punktach pomiarowych zgodnie z rysunkiem 18

| Element | Content (mass %) | | | | | | |
|---|---|---|---|---|---|---|---|
| | Spectrum 48 | Spectrum 49 | Spectrum 50 | Spectrum 51 | Spectrum 52 | Spectrum 53 | Spectrum 54 |
| O | 24.91 | 9.35 | 53.23 | 52.36 | 21.82 | 16.49 | 20.26 |
| Na | – | – | 0.74 | 0.14 | – | – | – |
| Mg | – | – | – | – | – | 3.27 | – |
| Al | 9.44 | 4.10 | 6.23 | 1.20 | 7.45 | 30.63 | 1.85 |
| Si | 6.89 | 2.19 | 31.28 | 44.79 | 3.72 | 2.08 | 1.29 |
| S | – | – | – | – | – | – | 0.32 |
| K | – | – | 3.74 | 0.20 | – | – | – |
| Ca | – | – | 1.03 | – | – | – | – |
| Ti | – | – | 0.72 | 0.40 | – | – | – |
| Fe | 22.95 | 78.61 | 3.02 | 0.91 | 11.96 | 32.98 | 5.31 |
| Cu | 35.82 | – | – | – | 55.05 | 7.02 | 70.97 |
| Zn | – | 5.74 | – | – | – | 7.52 | – |
| Total | 100.00 | 100.00 | 100.00 | 100.00 | 100.00 | 100.00 | 100.00 |

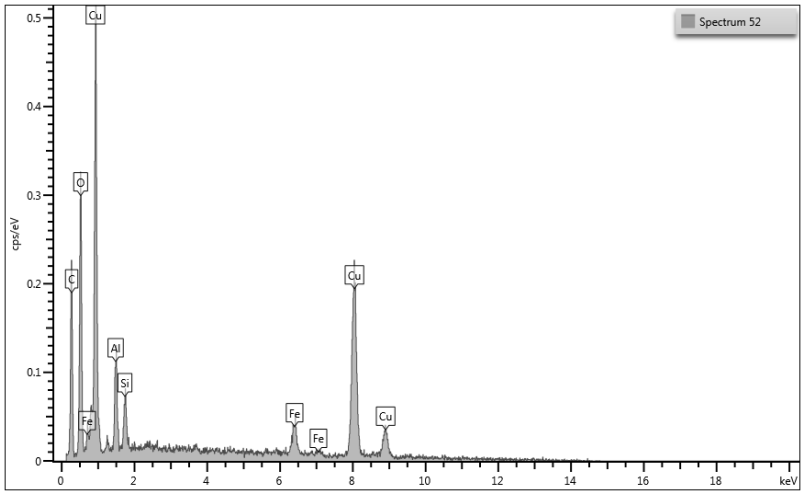


Fig. 19. EDS spectrum – spectrum 52, slag 2

Rys. 19. Widmo EDS – widmo nr 52, żużel nr 2

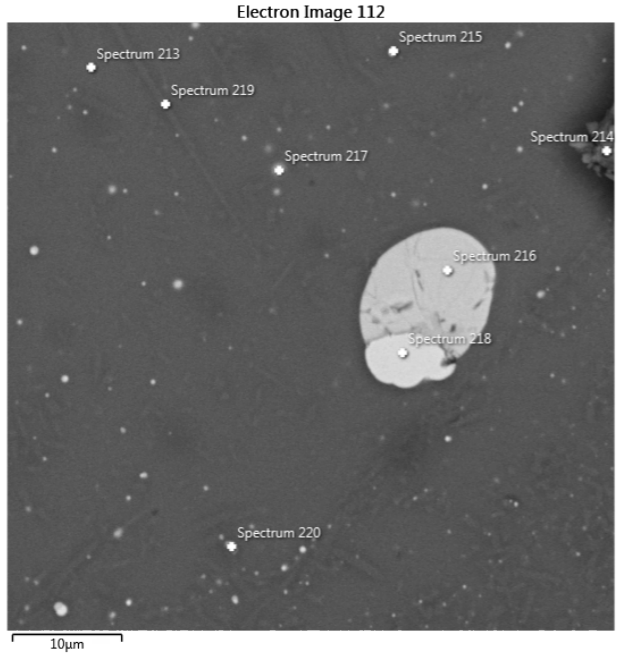


Fig. 20. Microphotograph 1 (BSE, magnification 5,000×) – slag 3

Rys. 20. Mikrofotografia 1 (BSE, powiększenie 5000×) – żużel nr 3

Table 8. Share of elements in measuring points according to Figure 20

Tabela 8. Skład pierwiastkowy w punktach pomiarowych zgodnie z rysunkiem 20

| Element | Content (mass %) | | | | | | | |
|---|---|---|---|---|---|---|---|---|
| | Spectrum 213 | Spectrum 214 | Spectrum 215 | Spectrum 216 | Spectrum 217 | Spectrum 218 | Spectrum 219 | Spectrum 220 |
| N | – | – | – | – | – | – | – | 4.17 |
| O | 48.21 | 47.37 | 44.57 | 45.72 | 37.73 | 30.28 | 48.53 | 47.88 |
| Na | 0.36 | 0.18 | 0.16 | – | 0.12 | – | – | 0.09 |
| Mg | 2.66 | 0.61 | 0.90 | – | 0.88 | – | 1.42 | 0.62 |
| Al | 11.38 | 3.14 | 5.39 | – | 3.42 | – | 25.91 | 4.28 |
| Si | 29.16 | 6.07 | 9.10 | – | 7.04 | 0.11 | 20.07 | 6.98 |
| P | – | – | – | – | 2.27 | 0.28 | – | – |
| S | 0.10 | 18.49 | 10.89 | 20.19 | 2.24 | – | – | 0.34 |
| K | 3.15 | 0.74 | 1.02 | – | 0.65 | – | 1.31 | 0.73 |

Table 8. cont.

Tabela 8. cd.

| Element | Content (mass %) | | | | | | | |
|---|---|---|---|---|---|---|---|---|
| | Spectrum 213 | Spectrum 214 | Spectrum 215 | Spectrum 216 | Spectrum 217 | Spectrum 218 | Spectrum 219 | Spectrum 220 |
| Ca | 4.19 | 22.82 | 0.99 | – | 0.71 | – | 1.62 | 0.65 |
| Ti | 0.79 | – | 1.08 | 3.54 | 0.22 | – | 1.14 | 31.81 |
| V | – | – | 0.31 | 0.48 | – | – | – | 1.59 |
| Cr | – | – | 0.27 | 0.73 | – | – | – | – |
| Mn | – | – | 0.79 | 1.41 | – | – | – | – |
| Fe | – | 0.59 | 24.52 | 27.93 | 44.73 | 69.33 | – | 0.86 |
| Total | 100.00 | 100.00 | 100.00 | 100.00 | 100.00 | 100.00 | 100.00 | 100.00 |

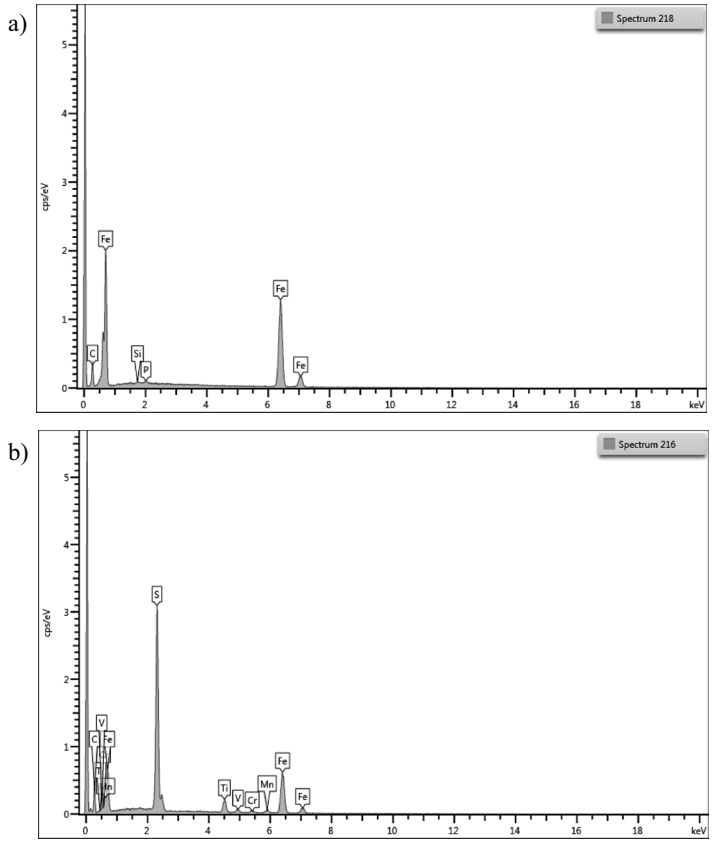


Fig. 21. EDS spectra – spectra 216 and 218, slag 3

Rys. 21. Widma EDS – widma nr 216 i 218, żużel nr 3

In the micro-area presented in Figure 22 (Figure 22, Table 9), there was cracking in the central part, filled with oxidized Fe compounds (points 182, 183, 190). Their form indicated that the cracking was refilled. Also, significant volumes of glaze with different chemical compositions were identified. In the bottom section of the micro-area, there was a clearly visible line between glaze 1 rich in Al, Si and Ca (point 180) and glaze 2 containing Si, Fe, Ca (point 189). Glaze 1 had isometric crystallites of spinel containing Mg, Fe and Al (points 179, 181). Spherical (point 186) or irregular (point 187) accumulations of iron sulfate could be identified around both types of glaze; moreover, glaze 2 had precipitates rich in Si and Fe.

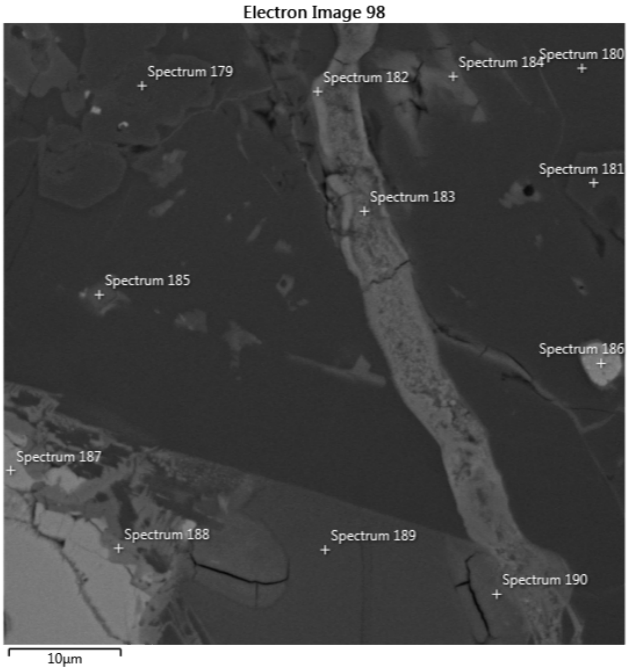


Fig. 22. Microphotograph 2 (BSE, magnification 5,000×) – slag 3

Rys. 22. Mikrofotografia 2 (BSE, powiększenie 5000×) – żużel nr 3

## 4. Complementary tests

As already mentioned, mineralogical and chemical research on slags requires the use of several complementary research techniques. Therefore, XRD tests were performed and the chemical composition of the tested slags was determined. The results are posted below.

Table 9. Share of elements in measuring points according to Figure 22

Tabela 9. Skład pierwiastkowy w punktach pomiarowych zgodnie z rysunkiem 22

| Element | Content (mass %) | | | | | | | | | | | |
|---|---|---|---|---|---|---|---|---|---|---|---|---|
| | Spectrum 179 | Spectrum 180 | Spectrum 181 | Spectrum 182 | Spectrum 183 | Spectrum 184 | Spectrum 185 | Spectrum 186 | Spectrum 187 | Spectrum 188 | Spectrum 189 | Spectrum 190 |
| O | 43.04 | 46.27 | 43.00 | 32.61 | 33.61 | 40.25 | 39.62 | 42.55 | 45.18 | 37.70 | 44.26 | 36.48 |
| Na | – | 0.37 | – | – | – | 0.28 | 0.44 | – | – | – | 0.32 | – |
| Mg | 10.49 | 0.12 | 10.45 | 0.55 | 1.04 | – | 0.99 | – | – | 1.24 | 1.21 | 0.77 |
| Al | 33.92 | 18.88 | 34.90 | 1.56 | 1.04 | 5.26 | 5.81 | 0.12 | – | 0.61 | 7.83 | 1.74 |
| Si | 0.44 | 21.11 | 0.10 | 2.24 | 2.84 | 9.84 | 12.57 | 0.12 | 0.09 | 12.89 | 23.66 | 5.12 |
| P | – | – | – | – | – | 0.14 | – | – | – | 0.49 | 0.25 | – |
| S | – | – | – | 1.16 | 2.21 | 4.01 | 1.88 | 16.69 | 20.20 | 0.92 | 0.14 | 3.79 |
| K | – | 0.47 | – | – | – | 0.63 | 0.57 | – | – | – | 4.53 | – |
| Ca | – | 12.19 | – | 0.59 | 0.46 | 1.83 | 3.08 | 0.24 | – | 2.72 | 7.27 | 0.27 |
| Ti | 0.46 | – | – | – | – | 4.23 | 0.44 | – | – | – | 2.24 | 2.23 |
| V | 0.44 | – | – | – | – | – | – | – | – | – | – | – |
| Mn | – | – | – | – | – | – | – | – | – | 0.73 | – | – |
| Fe | 11.21 | 0.59 | 11.56 | 61.30 | 58.79 | 33.54 | 34.59 | 39.71 | 34.52 | 42.69 | 8.28 | 49.60 |
| Ni | – | – | – | – | – | – | – | 0.57 | – | – | – | – |
| Total | 100.00 | 100.00 | 100.00 | 100.00 | 100.00 | 100.00 | 100.00 | 100.00 | 100.00 | 100.00 | 100.00 | 100.00 |

The identification of components using the X-ray diffraction method enabled determination of the types of specific phase components and their quantitative share in the composition of the slags. Additionally, the quantitative share of amorphous substance was determined.

The chemical compositions of the tested slags are presented in Table 11.

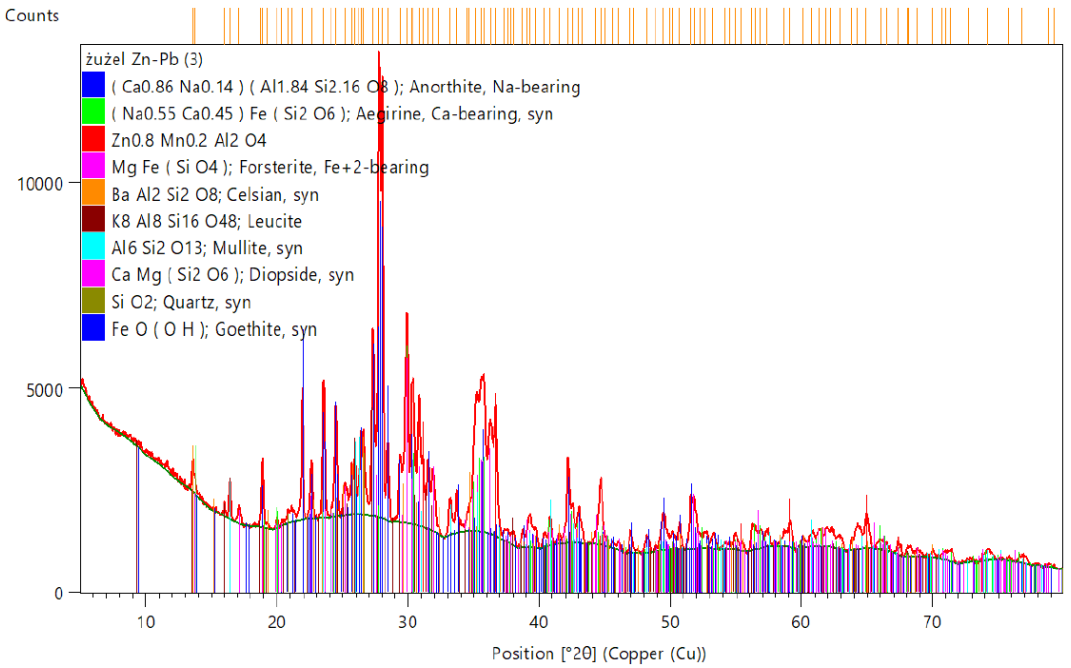


Fig. 23. Example diffraction pattern – slag 3

Rys. 23. Przykładowy dyfraktogram – żużel nr 3

## Discussion

The obtained test results using the SEM technique have shown that the phase composition of the analyzed Zn-Pb slags is significantly different. Within only one of the exposed slopes of the dump, the presence of three types of slag was found, characterized by different phase compositions. Such differentiation is related to changes in the composition of the metallurgical charge, which may have changed over fifty years of operation of the works. At the beginning, the main ingredient of the charge may have been red calamines, and later – sulfide ores. It cannot also be ruled out that no scrap was added to the charge, which could explain the presence of metallic iron precipitates in the slags. The preserved historical sources do not specify this information, there are also no documents from the works.

Table 10. Phase components and their quantitative share in the respective slag types

Tabela 10. Składniki fazowe i ich udział ilościowy w poszczególnych rodzajach żużli

| Sample No. | Phase composition | Formula | Quantitative share (%) | Standard deviation (%) |
|---|---|---|---|---|
| Slag 1 | Amorphous substance | – | 57.4 | 0.7 |
| | Anorthite | $Ca[Al_2Si_2O_8]$ | 21.2 | 0.3 |
| | Gahnite, solid solution 1 | $Zn^{2+}Al_2O_4$ | 0.7 | 0.1 |
| | Forsterite | $Mg_2[SiO_4]$ | 6.1 | 0.3 |
| | Leucite | $K[AlSi_2O_6]$ | 0.8 | 0.1 |
| | Mullite | $Al_6Si_2O_{13}$ | 1.6 | 0.1 |
| | Quartz | $SiO_2$ | 0.8 | 0.1 |
| | Goethite | FeOOH | 6.9 | 0.2 |
| | Hedenbergite | $CaFe[Si_2O_6]$ | 2.1 | 0.1 |
| | Gahnite, solid solution 2 | $Zn^{2+}Al_2O_4$ | 0.2 | 0.1 |
| | Spinel, solid solution | $MgAl_2O_4$ | 0.6 | 0.1 |
| | Perovskite | $CaTiO_3$ | 0.2 | 0.1 |
| | Lepidocrocite | (FeO(OH)) | 0.6 | 0.1 |
| | Barite | $BaSO_4$ | 0.9 | 0.1 |
| Slag 2 | Amorphous substance | – | 69.1 | 0.4 |
| | Anorthite | $Ca[Al_2Si_2O_8]$ | 13.0 | 0.2 |
| | Gahnite, solid solution | $Zn^{2+}Al_2O_4$ | 4.1 | 0.1 |
| | Mullite | $Al_6Si_2O_{13}$ | 1.8 | 0.1 |
| | Quartz | $SiO_2$ | 1.5 | 0.1 |
| | Spinel, solid solution | $MgAl_2O_4$ | 2.5 | 0.1 |
| | Tridymite | $SiO_2$ | 3.6 | 0.1 |
| | Cordierite | $Mg_2Al_3[AlSi_5O_{18}]$ | 0.3 | 0.1 |
| | Cristobalite | $SiO_2$ | 3.0 | 0.1 |
| | Augite | $(Ca,Na,Mg,Fe^{2+},Al,Ti)_2[(Si,Al)_2O_6]$ | 1.0 | 0.1 |
| Slag 3 | Amorphous substance | – | 58.6 | 0.6 |
| | Anorthite | $Ca[Al_2Si_2O_8]$ | 22.1 | 0.3 |
| | Acmite | $(Na,Ca,Fe)_6Zr[(OH,Cl)\|(Si_3O_9)_2]$ | 1.7 | 0.2 |
| | Gahnite, solid solution | $Zn^{2+}Al_2O_4$ | 1.5 | 0.1 |
| | Forsterite | $Mg_2[SiO_4]$ | 2.9 | 0.2 |
| | Celsian | $BaAl_2Si_2O_8$ | 0.4 | 0.1 |
| | Leucite | $K[AlSi_2O_6]$ | 1.3 | 0.1 |
| | Mullite | $Al_6Si_2O_{13}$ | 1.0 | 0.2 |
| | Diopside | $CaMg[Si_2O_6]$ | 9.4 | 0.3 |
| | Quartz | $SiO_2$ | 0.7 | 0.1 |
| | Goethite | FeOOH | 0.5 | 0.1 |

Table 11. Chemical composition of slags

Tabela 11. Skład chemiczny żużli

| Component | Content (mass %) | | |
|---|---|---|---|
| | Slag 1 | Slag 2 | Slag 3 |
| $SiO_2$ | 24.55 | 52.62 | 36.73 |
| Al | 8.39 | 11.44 | 13.47 |
| Ba | 0.27 | 0.43 | 0.79 |
| K | 1.14 | 1.75 | 1.78 |
| Mn | 0.31 | 0.30 | 0.28 |
| P | 0.04 | 0.06 | 0.14 |
| Pb | 0.32 | 0.08 | 0.14 |
| Sr | 0.08 | 0.03 | 0.12 |
| Ti | 0.36 | 0.45 | 0.55 |
| Zn | 2.29 | 3.21 | 1.09 |
| Zr | 0.01 | 0.01 | < 0.01 |
| Ca | 9.05 | 5.26 | 7.92 |
| Fe | 21.36 | 8.04 | 13.58 |
| Mg | 3.30 | 2.20 | 3.58 |
| Na | 0.32 | 0.26 | 0.28 |
| C | 5.76 | 0.29 | 2.84 |
| Total | 0.86 | 0.02 | 0.29 |

Nevertheless, it can be stated that the scanning electron microscopy observation technique used allowed the obtaining of precise research results that enabled the characterization of the phase composition of the slags. Using, inter alia, scanning electron microscopy (SEM/EDS), similar research was conducted by Ettler et al. (2002). Among the phase components in pyrometallurgical slag produced 100–150 years ago from lead–zinc ores in the smelting region of Příbram (Czech Republic), they distinguished clinopyroxene, melilite, olivine, spinel and glaze. No melilites were found in the slags from Bykowina, but groups of spinels and aluminosilicates were observed. Slags from Příbram spinels were represented primarily by gahnite (up to 19.9 wt% ZnO), while in the analyzed slags, in addition to gahnite, spinels rich in Al, Fe and Mg were found. In zinc slag from Świętochłowice, Puziewicz et al. (2007) distinguished above all silicates, mostly synthetic analogues of olivine, melilite, pyroxene, feldspars, willemite and of the oxides zincite and spinel-group phases.

Research on Zn-Pb slags from old dumps was also conducted by Warchulski et al. (2016); in the pyrometallurgical Zn-Pb slags from Katowice-Wełnowiec, they distinguished olivine, spinel series, melilite, clinopyroxene, leucite, nepheline and sulfides.

In order to supplement the obtained research results and to compare them with other research techniques, XRD analysis, which is also widely used in slag research, was performed. Based on XRD analysis, Espejel-García et al. (2022) conducted research on slags from an old smelter in Chihuahua, Mexico. The following components were described in these slags: hardystonite, melanotekite, sphalerite. In the tested slags from Bykowina, based on XRD analysis, it was found that in all the investigated slag types, the amorphous substance (glaze) was a major component; its share in slag 1 amounted to 57.4%, in slag 2 – 69.1% and in slag 3 – 58.6%. Other components were represented by silicate and oxide phases as well as secondary phases formed in the waste dump: sulfates and hydroxides. The crystalline phases in slag 1 included silicates: anorthite, forsterite, hedenbergite, and smaller amounts of: leucite, mullite and quartz. Among the oxides, there were solid solutions of gahnite and spinel, as well as perovskite. Slag 1 also had secondary phases represented by hydroxides: goethite and lepidocrocite, and sulfates – barite. In slag 2, the phase components were dominated by silicates and aluminosilicates, represented by: anorthite, mullite, quartz with its high-temperature variations – tridymite and cristobalite, as well as cordierite and augite. The oxides identified included solid solution of gahnite, solid solution of spinel. Slag 3 had numerous silicate and aluminosilicate phases; the most important being anorthite and diopside; the rest constituted about 1% and included acmite, forsterite, celsian, leucite, mullite, quartz. Oxide phases were represented by a solid solution of gahnite, whereas secondary phases were connected with the presence of goethite. In conclusion, XRD analysis confirmed the presence of components that were determined during microscopic observations, e.g. phases from the spinel and aluminosilicates group, mullite or barite. However, the presence of phases that were not observed during SEM tests, e.g. leucite and forsterite, was found. This can be explained by their occurrence in the form of tiny crystallites, unidentifiable during microscopic observations.

Analyzing the results of the chemical composition of tested slags, it was found that it reflects their phase composition. It could be stated that the major component of all the slags was $SiO_2$ (24.55–52.62%) accompanied by Al, Ca, Mg, K and the heavy metals Fe, Zn, and smaller volumes of Pb and Ti. The content of sulfur in the slags was quite low, it did not reach 1% in any sample and ranged between 0.22% and 0.86%.

## Conclusions

The following observations and conclusions were made based on the conducted research:

1. Studies using SEM are examples of the key research techniques which can be used to analyze and describe the components of metallurgical slags.

2. The conducted research revealed that the phase composition of the analyzed slags from the waste dump in Ruda Śląska – Bykowina was fairly diverse. The three types of slags identified by macroscopic observations; furthermore, microscope examination not only had different external characteristics but also different crystallite inventory. The common characteristic for all three types of slags was the major glaze content exceeding 50% of content of all slag components. Similar results regarding the glaze content in slags were recorded for the waste from the heap in Ruda Śląska – Wirek. The glaze that was the dominant component was also characterized by a rich chemical composition, with Si, Al, K, Na and P, as well as S and heavy metals: As, Cd, Cu, Mn, Fe, Pb, Zn and Ti. It is also interesting that in the waste dump in Wirek, completely vitrified waste was discovered in the slags, this was mainly glaze with minor metallic precipitates and calcium silicate crystal nuclei (Jonczy 2022).
3. Observations using secondary electrons (SE) enabled characteristics of the surface morphology of the slags in question as well as morphology of its components. Generally, based on this, two areas with differentiated morphology were identified in the slags. There were fragments with coarse structure and visible crystallites of phase components and vitrified material with smooth, non-fractured surface and numerous regular-, round-shaped pores. The presence of areas with different structures indicates a diverse and two-step process of cooling the slag. The material containing crystallites cooled at a slower rate. This allowed initiation of the crystallization of the phase components, whereas the vitrified sections were formed as a result of rapid cooling of the slag with its simultaneous degassing which is exhibited by the presence of numerous pores.
4. Based on the SEM observations, it can be concluded that the main component of the tested slags is glaze, but its chemical composition in the three distinguished varieties is slightly different. In the glaze of slag no. 1, three elements occur in the largest quantities – Si (over 20%), Ca (12–19%) and Al (14–19%). The glaze from slag no. 2 is dominated by Si (over 30%), next to which, with several %, occur Al, K, Fe, Ca. Slag no. 3 glaze is generally rich in two elements – Al and Si.
5. In slag no. 1, among the silicate and aluminosilicate phases, fine crystallites of Fe-Mg silicates have been distinguished; in slag no. 2, aluminosilicate crystallites rich In Ti and K dominated, whereas in slag no 3 crystallites with needle like habit rich in Al and Si have been found. Their morphology and chemical composition indicate the presence of mullite. Mullite belongs to the group of island silicates which additionally contain another anion, [OH]- and F- in the case of mullite. This mineral is one of the products of kaolinite transformation, it crystallizes at 1000°C, is very durable and decomposes into corundum and $SiO_2$ alloy at 1800°C. It had a typical fuel habit visible in SEM microphotographs (Figure 20, point 219). The presence of mullite in the slags was connected with the charge material, especially fluxing agents, as clay materials are often admixtures in carbonate rocks. In nature, mullite is a rare mineral,

it was identified in clay rocks sintered during underground fires of coal deposits (Duval et al. 2008, Mindat.org).

6. Of the oxide phases, spinels dominate in all slag types. They were represented by proper spinel, which forms polymorphic series with hercynite, and gahnite ($ZnAl_2O_4$). Theoretically, proper spinel contains 28.2% MgO and 71.8% $Al_2O_3$, but numerous isomorphic admixtures of Cr, Zn, Fe and Mn can be often found in its inner structure, which leads to the formation of many variations of this mineral with different macroscopic features. In the slags tested, besides Mg and Al, proper spinel contained major admixtures of Fe as well as hercynite – spinel rich in Fe and Al. Gahnite, identified in all the analyzed slags is a zinc spinel representing zinc and aluminum oxide. This mineral is rarely encountered in nature and is typical for contact metamorphized limestones and metasomatic ore veins and deposits (Mindat.org). Its presence was pronounced in slag 2. The gahnite crystals were well developed, idiomorphic and had a characteristic octahedral habit (Figure 22; points 123, 127).
7. The pores identified in slags were often filled with recrystallizing minerals represented by iron oxide (hematite) and also barite.
8. Additional tests using the XRD technique confirmed the presence of the components determined during microscopic observations and also showed the presence of other phases. This indicates that research on the phase composition of slags requires the use of several complementary research techniques.

## REFERENCES

Ali et al. 2023 – Ali, A., Zhang, N. and Santos, R.M. 2023. Mineral characterization using Scanning Electron Microscopy (SEM): A Review of the Fundamentals, Advancements, and Research Directions. *Applied Sciences* 13(23), DOI: 10.3390/app132312600.

Bleiwas, D.I. and DiFrancesco, C. 2010. Historical zinc smelting in New Jersey, Pennsylvania, Virginia, West Virginia, and Washington, D.C., with estimates of atmospheric zinc emissions and other materials. Open-File Report 2010–1131, U.S. Geological Survey, Reston, Virginia.

Cabała et al. 2008 – Cabała, J., Żogała, B. and Dubiel, R. 2008. Geochemical and geophysical study of historical Zn-Pb ore processing waste dump areas (Southern Poland). *Polish Journal Environmental Study* 17(5), pp. 693–700.

Duval et al. 2008 – Duval D.J., Risbud S.H., and Shackelford J.F. 2008. *Chapter 2 – Mullite in Ceramic and Glass Materials: Structure, Properties and Processing*, Shackelford J.F. and Doremus R.H. (eds.), Springer.

Dworak, J.S. 1995. *Karol Godula*. Państwowy Instytut Naukowy, Instytut Śląski w Opolu, Związek Górnośląski, koło Nowy Bytom w Rudzie Śląskiej, Opole-Ruda Śląska (*in Polish*).

Dworak, J.S. and Ratka, A. 1985. *Ruda Śląska – przewodnik*. Towarzystwo Przyjaciół Miasta Rudy Śląskiej, Oddział Miejski Polskiego Towarzystwa Turystyczno-Krajoznawczego w Rudzie Śląskiej, Ruda Śląska (*in Polish*).

Espejel-García et al. 2022 – Espejel-García, D., Espejel-García, V.V. and Villalobos-Aragón, A. 2022. Chemical characterization of slags from an old smelter in Chihuahua, Mexico. *Journal of Minerals and Materials Characterization and Engineering* 10(6), pp. 461–476, DOI: 10.4236/jmmce.2022.106033.

Ettler et al. 2001 – Ettler, V., Legrande, O., Bodenan, F. and Touray, J.C. 2001. Primary phases and natural weathering of old lead-zinc pyrometallurgical slag from Príbram, Czech Republic. *The Canadian Mineralogist* 39(3), pp. 873-888, DOI: 10.2113/gscanmin.39.3.873.

Ettler et al. 2009 – Ettler, V., Červinka, R. and Johan, Z. 2009. Mineralogy of medieval slags from lead and silver smelting (Bohutín, Příbram District, Czech Republic): towards estimation of historical smelting conditions. *Archeometry* 51(6), pp. 987–1007, DOI: 10.1111/j.1475-4754.2008.00455.x.

Jonczy, I. 2016. Microstructures of metallurgical slags. *Archives of Metallurgy and Materials* 61(1), pp. 61–66, DOI: 10.1515/amm-2016-0015.

Jonczy, I. 2018. The use of selected structural tests in the determination of phase composition of industrial wastes based on the example of Zn-Pb slags. *IOP Conference Series: Materials Science and Engineering*. [On-line:] https://iopscience.iop.org/article/10.1088/1757-899X/427/1/012001/pdf [Accessed: 2024-01-05].

Jonczy, I. 2022. Phase and chemical composition of historical Zn-Pb slag from the dump in Ruda Śląska (Silesian Province, southern Poland). *Acta Montanistica Slovaca* 27(1), pp. 70–83, DOI: 10.46544/ams.v27i1.06.

Jonczy, I. and Stanek, J. 2013. Phase composition of metallurgical slag studied by Mössbauer spectroscopy. *Nukleonika International Journal of Nuclear Research* 58(1), pp. 127–131.

Kicińska, A. 2021. Physical and chemical characteristics of slag produced during Pb refining and the environmental risk associated with the storage of slag. *Environ Geochem Health* 43(7), pp. 2723–2741, DOI: 10.1007/s10653-020-00738-5.

Koga et al. 2021 – Koga, D., Kusumi, S., Shibata, M. and Watanabe, T. 2021. Applications of Scanning Electron Microscopy using secondary and backscattered electron signals in neural structure. *Front. Neuroanat.* 15, DOI: 10.3389/fnana.2021.759804.

Kucha et al. 1996 – Kucha, H., Martens, A., Ottenburgs, R., De Vos, W. and Viaene, W. 1996. Primary minerals of Zn -Pb mining and metallurgical dumps and their environmental behavior at Plombières, Belgium. *Environmental Geology* 27, pp. 1–15, DOI: 10.1007/BF00770598.

Lin et al. 2015 – Lin, W., Xiao, T., Zhou, W. and Ning, Z. 2015. Pb, Zn, and Cd distribution and migration at a historical zinc smelting site. *Polish Journal of Environmental Studies* 24(2), pp. 575–583, DOI: 10.15244/pjoes/26107.

Liu et al. 2010 – Liu, F., Wu, J., Chen, K. and Xue, D. 2010. *Morphology study by using Scanning Electron Microscopy.* [In:] *Microscopy: Science, Technology, Applications and Education*, Méndez-Vilas, A. and Díaz J. (eds.), pp. 1781–1792.

Łydżba-Kopczyńska et al. 2024 – Łydżba-Kopczyńska, B., Walczak, M., del Hoyo Meléndez, J. and Garbacz-Klempka, A. Skaningowa mikroskopia elektronowa z analizatorem EDS – UWr. [On-line:] http://www.e-rihs.pl/index.php/sem-eds-2/skaningowa-mikroskopia-elektronowa-z-analizatorem-eds-uwr/ [Accessed: 2024-01-05].

Mindat.org. [On-line:] https://www.mindat.org/min-2806.html [Accessed: 2024-01-05].

Nadeau, G. and Herguth, W.R. 2004. Applying SEM-EDS to Practical Tribology Problems. [On-line:] https://www.machinerylubrication.com/Read/628/sem-eds-tribology [Accessed: 2024-01-05].

Nocoń et al. 2023 – Nocoń, M., Korus, I., Loska, K. 2023. Quantitative and qualitative analysis of slags from zinc and lead metallurgy. *Archives of Environmental Protection* 49, pp. 26–37, DOI: 10.24425/aep.2023.147326.

Pazdur, J. (ed.) 1961. *Zarys dziejów górnictwa na ziemiach polskich*. Tom I i II, Katowice: Wydawnictwo Górniczo-Hutnicze (*in Polish*).

Popiołek, K. 1965. *Górnośląski przemysł górniczo-hutniczy w drugiej połowie XIX wieku*. Katowice-Kraków: Śląski Instytut Naukowy w Katowicach (*in Polish*).

Puziewicz et al. 2007 – Puziewicz, H., Zainoun, K. and Bril, H. 2007. Primary phases in pyrometallurgical slags from a zinc-smelting waste dump, Świętochłowice, Upper Silesia, Poland. *The Canadian Mineralogist* 45(5), pp. 1189–1200, DOI: 10.2113/gscanmin.45.5.1189.

Ruda Śląska Location 2023. [Online] https://pl.m.wikipedia.org/wiki/Plik:Dzielnice_Rudy_%C5%9Al%C4%85skiej.svg [Accessed: 2023-12-12].

Warchulski et al. 2016 – Warchulski, R., Gawęda, A., Janeczek, J. and Kądziołka-Gaweł, M. 2016. Mineralogy and origin of coarse-grained segregations in the pyrometallurgical Zn-Pb slags from Katowice-Wełnowiec (Poland). *Mineralogy and Petrology* 110(5), pp. 681–692, DOI: 10.1007/s00710-016-0439-1.

Wu et al. 2017 – Wu, J., Wang, L. and Meng, L. 2017. Analysis of mineral composition and microstructure of gravel aggregate based on XRD and SEM. *Road Materials and Pavement Design* 18(1), pp.139–148, DOI: 10.1080/14680629.2017.1329869.

Zdera, J. 2013. *Metoda scanningowej mikroskopii elektronowej innowacją w naukach mineralogicznych*. [On-line:] http://laboratoria.net/artykul/13741.html [Accessed: 2024-01-05].

## THE USE OF SCANNING ELECTRON MICROSCOPY IN THE STUDY OF THE COMPONENTS OF ZN-PB SLAGS ON THE EXAMPLE OF SLAGS FROM THE DUMP IN BYKOWINA (RUDA ŚLĄSKA)

Keywords

scanning Electron Microscopy, metallurgical slag, phase composition

Abstract

Scanning electron microscopy (SEM) enables the obtaining of high-resolution images of sample surfaces by recording secondary electrons (SE) or backscattered electrons (BSE) characterized by depth of field and high resolution. Observations using scanning electron microscopy are widely used in many fields of science. The authors show that scanning electron microscopy is also one of the key technique used in the study of the metallurgical slags components. The research was performed for three types of slag following the production of Zn and Pb collected from an old dump in Ruda Śląska – Bykowina. The slag components were identified, morphology and chemical composition of the crystalline phases were characterized and the chemical composition of glaze was determined. Based on observations using secondary electrons, two areas with diverse morphology were identified in slag resulting from the production of cast iron: fragments with coarse structure and visible crystallites of phase components, and a vitrified material with a smooth, non-fractured surface and numerous regular- and round-shaped pores. It was found that in the surroundings of the dominant glaze (rich mainly in Si, Ca and Al) in all types of slags, well-developed crystals of phase components can be distinguished: in slag no. 1, these are Fe-Mg silicates; in slag no. 2, they are aluminosilicates of Ti and K; in slag no. 3, the presence of fine needle-shaped crystals containing Al and Si was found, which indicates the presence of mullite. During the storage in the dumping ground, numerous secondary minerals crystallize in the pores of the slag. Pores are the remains of the degassing of the slag melt during its cooling – hematite and barite were identified among them.

## WYKORZYSTANIE SKANINGOWEJ MIKROSKOPII ELEKTRONOWEJ W BADANIACH SKŁADNIKÓW ŻUŻLI ZN-PB NA PRZYKŁADZIE ŻUŻLI ZE ZWAŁOWISKA W BYKOWINIE (RUDA ŚLĄSKA)

Słowa kluczowe

skaningowa mikroskopia elektronowa, żużel hutniczy, skład fazowy

Streszczenie

Skaningowa mikroskopia elektronowa (SEM) pozwala uzyskać wysokorozdzielcze obrazy powierzchni próbek za pomocą rejestracji elektronów wtórnych (SE) lub elektronów wstecznie rozproszonych (BSE), charakteryzujące się głębią ostrości oraz wysoką rozdzielczością. Obserwacje przy wykorzystaniu skaningowej mikroskopii elektronowej znajdują szerokie zastosowanie w wielu dziedzinach nauki, autorzy pokazali, że skaningowa mikroskopia elektronowa to także jedna z kluczowych technik wykorzystywana w badaniach składników budujących żużle hutnicze. Badania

przeprowadzono dla trzech rodzajów żużli po produkcji Zn i Pb pobranych ze starego zwałowiska w Rudzie Śląskiej – Bykowinie. Dokonano identyfikacji składników budujących żużle, scharakteryzowano morfologię faz krystalicznych, oznaczono ich skład chemiczny, jak również skład chemiczny szkliwa. Na podstawie przeprowadzonych obserwacji w żużlach wyróżniono dwa obszary o zróżnicowanej morfologii; obok fragmentów o chropowatej strukturze z widocznymi zarysami krystalitów składników fazowych, wyróżniono zeszklony materiał o gładniej, niespękanej powierzchni, w obrębie którego występują liczne pory o regularnych, okrągłych kształtach. Stwierdzono, że w otoczeniu dominującego szkliwa (bogatego przede wszystkim w Si, Ca i Al), we wszystkich rodzajach żużli można wyróżnić dobrze wykształcone kryształy składników fazowych: w żużlu nr 1 są to krzemiany Fe-Mg, w żużlu nr 2 – glinokrzemiany Ti i K, natomiast w żużlu nr 3 stwierdzono obecność drobnych kryształów o pokroju igiełkowym zawierających Al i Si, co wskazuje na obecność mullitu. Podczas składowania na zwałowisku, w porach żużli, stanowiących pozostałość po odgazowania stopu żużlowego w trakcie jego chłodzenia, licznie krystalizują minerały wtórne – zidentyfikowano wśród nich hematyt oraz baryt.